

http://pubs.acs.org/journal/aelccp

Insights into Indigo K⁺ Association in a Half-**Slurry Flow Battery**

Xiao Wang, Jingchao Chai,* Shu Zhang, Bingbing Chen, Ashwin Chaturvedi, Guanglei Cui, and Jianbing Jimmy Jiang*



Downloaded via UNIV OF CINCINNATI on July 27, 2023 at 18:57:04 (UTC). See https://pubs.acs.org/sharingguidelines for options on how to legitimately share published articles.

Cite This: ACS Energy Lett. 2022, 7, 1178-1186



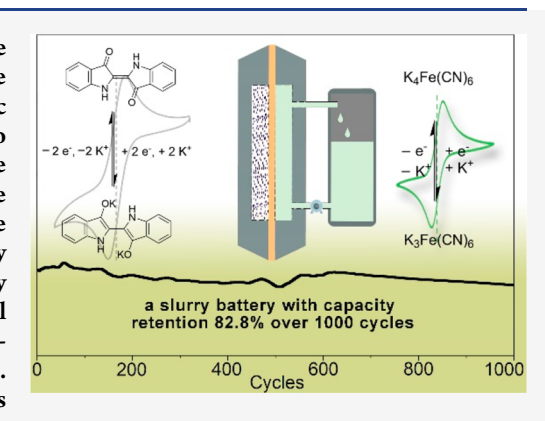
ACCESS I

III Metrics & More

Article Recommendations

Supporting Information

ABSTRACT: Potassium-ion batteries (PIBs) are promising energy storage devices owing to the abundance and low cost of potassium. However, the development of PIBs is still in its infancy owing to the poor kinetic diffusivity, limited capacity, and severe side reactions. It is imperative to explore new materials to address the issues of capacity, stability, and cycle life in PIBs. Here, we present a hybrid slurry/flow battery utilizing redox-active organic materials for K+ storage, wherein the indigo slurry serves as the anolyte and $K_4Fe(CN)_6$ solution serves as the catholyte. This battery presented a cycle life of 1000 cycles with a capacity of 18.4 Ah/L and capacity retention of ~83%. Voltammetry measurements and density functional theory calculations indicated that the redox activity of indigo involves a onestep, double-electron process, instead of a two-step, single-electron process. This work provides new insights into the application of organic compounds as association materials for PIBs.



ith the ever-growing energy consumption, the search for renewable and nonpolluting energy has become a significant strategic plan worldwide. The transition from fossil fuels to renewable energy, such as solar and wind, is expected to reduce the dependence on traditional fossil fuels. 1,2 However, most renewable energy sources share a key technical barrier, which is the mismatch between energy production and demand for energy consumption. Fortunately, the developed energy storage devices play an important role in peak load shifting of electricity utilization in smart grids.³⁻⁶ Energy storage devices can be classified into two categories: solid-state batteries and liquid-flow batteries. As a representative of solid-state batteries, lithium-ion batteries (LIBs) have been widely used in portable electronics and electric vehicles owing to their high energy density and superior cycling stability. 7-9 To achieve higher energy density and longer cycle life of solid-state batteries, post-lithium-ion batteries, such as sodium-ion batteries, 10,11 magnesium-ion batteries, 12,13 and potassium-ion batteries (PIBs), 14,15 have been proposed and researched. Compared with magnesium and lithium, potassium is more abundant in the earth's crust (2-3%). In addition, the Stokes radius of solvated potassium molecules is smaller than that of sodium or lithium for a given solvent, 19,20 which leads to higher mobility of K+ than Li+ and Na+ ions, allowing for high-rate performance. Redox flow batteries (RFBs) are representative liquid-flow batteries that store energy in liquid redox electrolytes. $^{21-32}$ As one of the

most successful representatives of RFBs, all-vanadium RFBs have reached a scale of up to MW/MWh. 33,34 Owing to the low cell operation voltage and limited active material concentration, the energy density of RFBs (25 Wh/L) is lower than that of commercial LIBs (800 Wh/L).35,36 However, the unique configuration of RFBs, where the redox-active materials are stored in external reservoirs, enables upscaling of power and energy independently. Both the energy and power density of RFBs are dependent on the solubility of the electroactive materials. 37,38 With the development of organic-based RFBs, wherein organic molecules serve as redox species, this solubility issue becomes increasingly severe. Although molecular engineering is effective in increasing the solubility of organic redox materials, complicated and tedious chemical modification processes are inevitable.

As an electrochemically active organic compound, indigo (Figure 1) has been used in different electrochemical energy storage systems. Sodium sulfonated indigo has been successfully used in lithium organic batteries and sodium organic batteries.³⁹⁻⁴² Zhu et al. increased the solubility of indigo

Received: January 21, 2022 Accepted: February 23, 2022 Published: February 28, 2022





Figure 1. Indigo and derivatives in electrochemical energy storage systems.

carmine to 0.76 M under harsh, strongly acidic conditions by replacing the metal ions with protons in RFBs. 43 Despite a few successful cases, indigo and its derivatives still suffer from extremely low solubility in most common solvents (acetonitrile, carbonate, N,N-dimethylformamide, and water) for flow battery applications.⁴⁴ Although the high insolubility largely limits its application in solution-based batteries, this property enables the use of indigo as a slurry electrode in aqueous electrolytes. Redox slurry batteries, in which the liquid electrolytes used in RFBs are replaced with stable, nonsettling suspended active materials, are promising for addressing the solubility issue of electroactive materials in electrolytes. Owing to the abundance of insoluble organic electroactive materials, slurry batteries are advantageous in reducing cost and overcoming solubility limitations. 48,49 Moreover, the application of slurry electrolytes mitigates the crossover issue, 45,46,50,51 resulting in a wider selection of battery separators, thus reducing the cost of the entire energy storage system. 46,52-54 Based on these advantages, slurry batteries typically present high Coulombic efficiency and excellent cycling stability, where these features are conducive to the development of large-scale high-energy-density energy storage

In this work, we present an aqueous potassium-ion slurry battery using indigo as the electron carrier and $K^{\scriptscriptstyle +}$ association material. Paired with aqueous $K_4 Fe(CN)_6$ catholyte, the asfabricated battery shows a high capacity of 18.4 Ah/L and maintains a high-capacity retention of 82.8% after 1000 cycles, corresponding to 99.98% per cycle. The combination of voltammetry, cycling performance analysis, and density functional theory (DFT) calculations demonstrates the viability of the slurring strategy and the use of indigo as a potassium association material.

The solubility of indigo was tested in pure water in an attempt to prepare a 1 mM solution. The extremely low solubility (<1 mM) of indigo is attributed to the strong intermolecular and intramolecular hydrogen bonds observed in indigo crystals.⁵⁵ The solubility of the reduced indigo was studied by bulk electrolysis of immobilized indigo on a carbon paper electrode, followed by cyclic voltammetry (CV) analysis of the postelectrolysis solution (Figure S1). No obvious color change was found during the whole electrolysis process (Figure S1A), suggesting no substantial leaching of indigo from the electrode, given the dark color the indigo. The postelectrolysis electrolyte was also subjected to CV using a glassy carbon electrode, and no redox features were observed, indicating that indigo at different charge states is not soluble in the electrolyte (Figure S1B). The electrochemical characteristics of insoluble indigo were first studied by CV. Indigo displayed a reversible

redox potential of -0.64 V vs Ag/AgCl, with a current peak-height ratio ($i_{\rm p,ox}/i_{\rm p,red}$) of 1.04 in 0.5 M KCl in H₂O/TEGDME (95:5) electrolyte using indigo-deposited carbon paper as the working electrode (Figure 2A). To study the

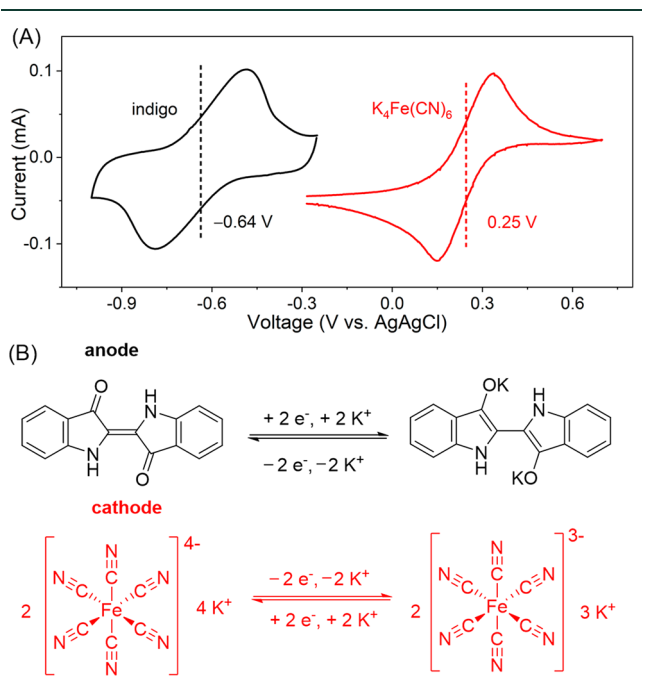


Figure 2. (A) Cyclic voltammograms of 5.0 mM $K_4Fe(CN)_6$ on a glassy carbon electrode and a dried indigo suspension on carbon paper at the scan rate 50 mV/s in 0.1 M KCl in $H_2O/TEGDME$ (95:5). (B) Redox half-reactions of indigo and $K_4Fe(CN)_6$.

stability of indigo, electrochemically reduced indigo was generated and stored at room temperature, and intermittent CV measurements were conducted. Highly consistent, reversible voltammograms were observed during storage for 142 h (Figure S2), indicating the electrochemical persistence of indigo in the reduced state. When paired with a well-studied catholyte, $K_4Fe(CN)_6$, with a redox potential of 0.25 V vs Ag/AgCl in 0.5 M KCl in $H_2O/TEGDME$ (Figure 2A), the indigo-based half-slurry/half-flow battery presented a theoretical potential of 1.1 V (Figure S3). The half-battery reaction is also shown in Figure 2B, where $K_4Fe(CN)_6$ is single-electron active and indigo is double-electron active. In this battery, the indigo slurry and $K_4Fe(CN)_6$ solution served as the negative and positive potassium-storing materials, respectively.

To further investigate the interaction of K⁺ with indigo, the probability distribution of the molecular electrostatic potential of indigo in different charge states (indigo, indigo-, and indigo²⁻) was calculated using Gaussian software,⁵⁶ which showed that the electron density was uniformly distributed throughout the structure of neutral indigo due to π conjugation and molecular symmetry (Figure 3A). For charged indigo molecules (indigo and indigo 1), the oxygen atoms presented a more negative electrostatic potential than the other atoms, suggesting that the electrophilic C=O group of indigo tends to coordinate with the K⁺ cation. To verify the reaction path of indigo during the charging/discharging process, the free energy of indigo in different charge states was calculated by DFT (Figure 3B and C). The one-electron reduction of indigo increased the free energy by 36.79 kcal/mol, which is three times higher than that of the two-electron reduction

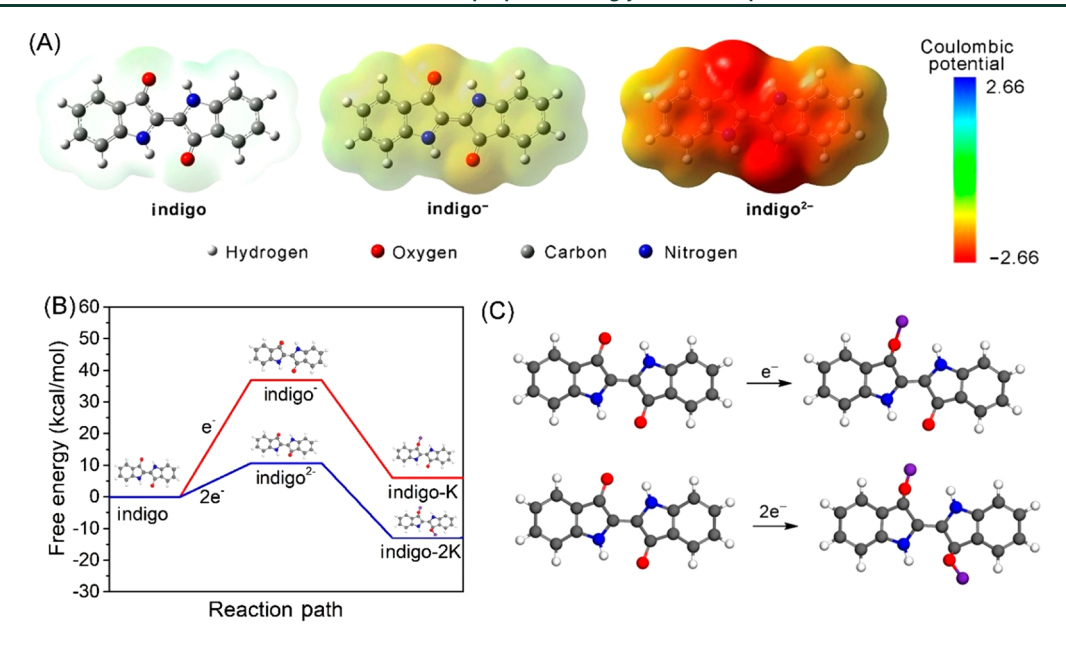


Figure 3. (A) Molecular electrostatic potentials of indigo, indigo⁻, and indigo²⁻. The electron-rich and electron-deficit regimes of the molecules are represented by red and blue, respectively. (B) Change in free energy. (C) Reaction path of indigo during single-electron and double-electron reactions.

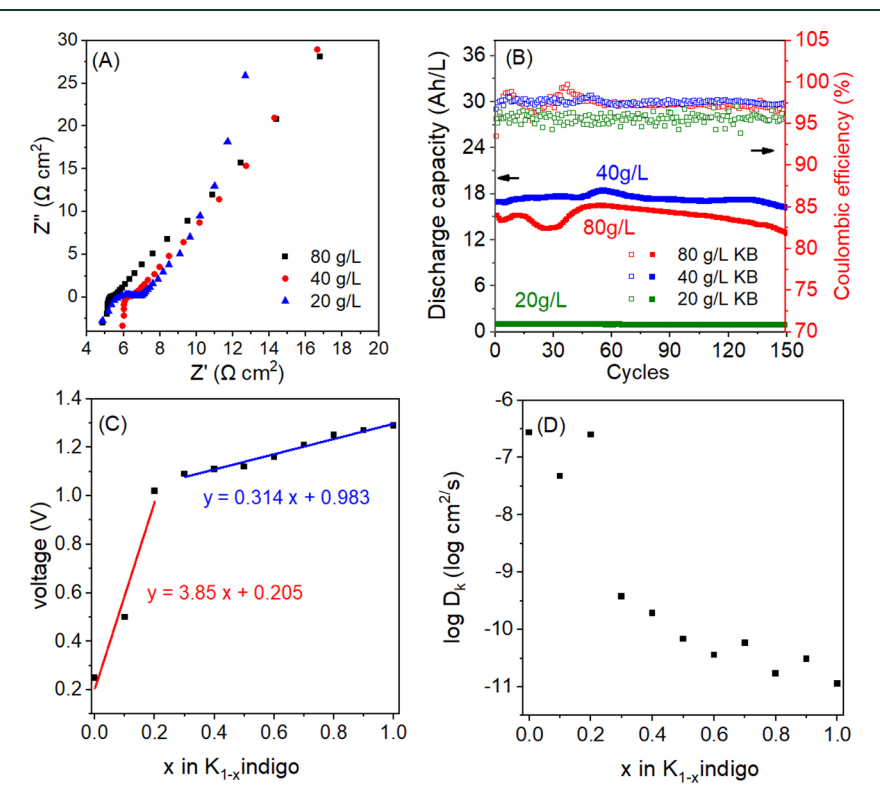


Figure 4. (A) Electrochemical impedance spectroscopy with various KB ratios (20, 40, and 80 g/L). (B) Long-term cycling properties of a 1.0 M indigo/ K_4 Fe(CN)₆ battery with different Ketjen black (KB) loadings. (C) Coulometric titration: voltage as a function of degree of K^+ association in indigo. (D) Diffusion coefficient of K^+ on the surface of an indigo slurry vs degree of K^+ association.

process, indicating that the one-electron reduction of indigo is less energetically favorable than the two-electron reaction. In addition, after adsorption of K^+ , the free energy of 2K-indigo was 12.98 kcal/mol lower than that of neutral indigo, further confirming the predominance of the two-electron reaction pathway. This finding provides evidence that the redox reaction of indigo is a one-step, two-electron process rather than a two-step, one-electron process.

The insulating nature of organic compounds typically poses conductivity challenges for battery applications yet can be mitigated by mixing these compounds with conductive carbon materials, such as Ketjen black (KB). This strategy has been successfully adopted in slurry and solid organic-based energy storage systems. 52,57-59 Because of the poor electronical conductivity of indigo powder, KB is introduced into the indigo slurry to enhance the conductivity of the slurry (see

ACS Energy Letters http://pubs.acs.org/journal/aelccp Letter

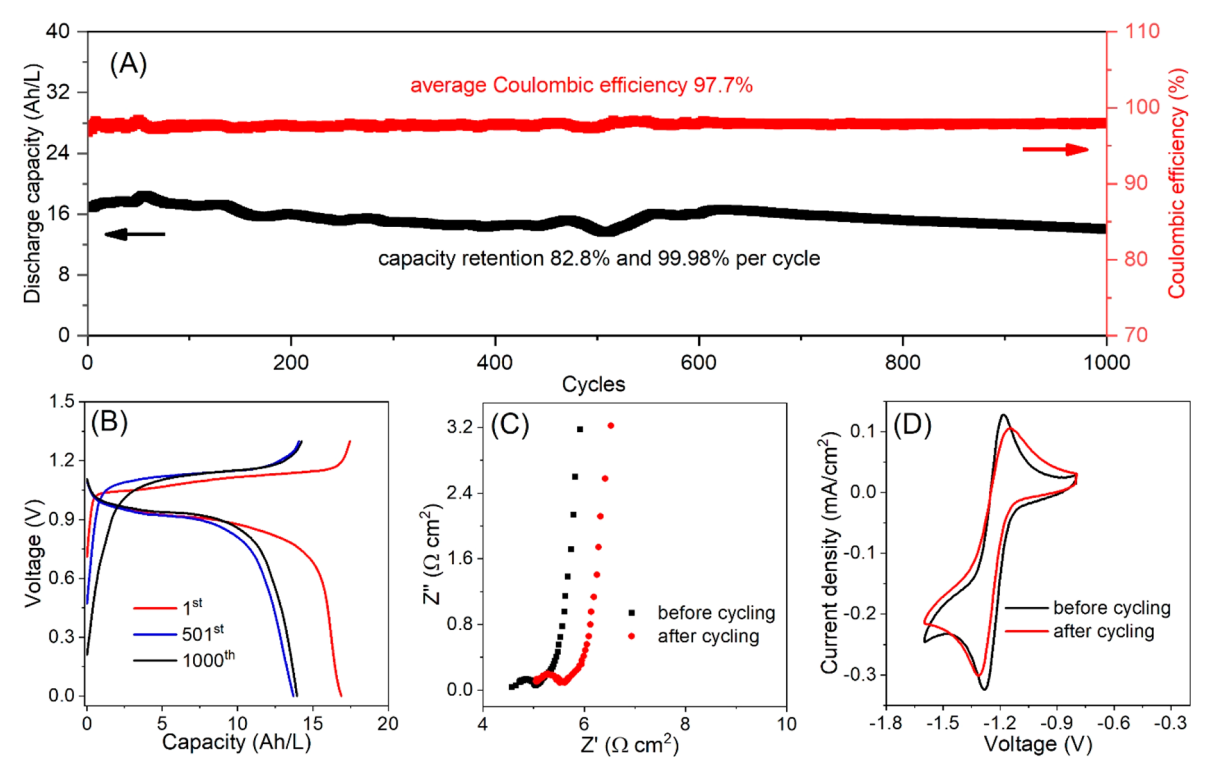


Figure 5. Long-term cycling properties of the 1.0 M indigo/ K_4 Fe(CN) $_6$ battery. (A) Discharge capacity and Coulombic efficiency over 1000 cycles. (B) Charge/discharge profiles at different cycle numbers. (C) Electrochemical impedance spectra before and after cycling. (D) CV scans of indigo before cycling and after cycling. The indigo/KB suspension electrolytes were dried at 60 °C for 12 h, after which the 5.0 mg dried indigo/KB electrolytes were soaked in 5.0 mL of DMSO for 2.0 h to get a clear supernatant liquid. Tetrabutylammonium hexafluorophosphate (0.1 M) was used as the supporting salt.

Experimental Section in the Supporting Information for details and Figure S4). Indigo (1.0 M) and different proportions of KB (20, 40, or 80 g/L) were mixed with 2.0 mL 1.0 M KCl in a H₂O/tetraethylene glycol dimethyl ether (TEGDME, 95:5 by volume) stock solution to prepare a homogeneous slurry. The use of TEGDME improves the dispersion of indigo in an aqueous medium to afford a uniformly distributed indigo slurry. The slurries with various KB concentrations (20, 40, and 80 g/L) were screened using electrochemical impedance spectroscopy (EIS), as shown in Figure 4A. An insignificant difference in the internal resistance (R_{Ω}) was observed (maximum 0.7 Ω cm²). However, the interface resistance of the 20 g/L sample was higher than that of the other two samples. Subsequently, batteries with different KB ratios were prepared (schematics of the battery model are shown in Figures S5 and S6) and the long-term cycling was evaluated. As shown in Figure 4B, the indigo utilization of the 20 g/L-KB battery (1.4 Ah/L) was low among all those batteries (1.0 M battery with the theoretical capacity of 53.6 Ah/L), presumably due to the insufficient amount of conductive material. In contrast, the 40 g/L- and 80 g/L-KB batteries demonstrated superior energy utilization, capacity retention, and Coulombic efficiency, suggesting that a KB slurry loading of 40 g/L and 80 g/L facilitated the construction of effective electron conducting networks within the slurry system. Compared with the 80 g/L-KB battery, the battery with 40 g/L of KB performed slightly better in terms of the cycle performance test: 0.3% higher average Coulombic efficiency (97.3% vs 97.6%) and 11.8% higher 150-cycle capacity retention (84.0% vs 95.8%). In addition, the use of fewer additive components increases the

energy density of the system; thus, a KB loading of 40 g/L was employed for subsequent studies.

For PIBs, the diffusion of K⁺ on the electrode surface has a significant effect on the battery performance, including the cyclability and rate performance. 60 In this indigo slurry system, the K⁺ diffusion kinetics were investigated using EIS.^{61–64} By fitting the real impedance (Z') and the square root of the angular frequency in the low-frequency region, the Warburg coefficient was obtained (Equation S1 and Figure S7). 65,66 In parallel, Coulometric titration was used to determine the slope of the open-circuit voltage vs K^+ concentration (x) relation at each x value (Figure 4C), which affords the K⁺ diffusion values using Equation S2 (Figure 4D).⁶⁷ At the initial stage of K⁺ intercalation, the entire slurry system showed high diffusion coefficients ($\sim 10^{-7}$ cm²/s). As K⁺ association progressed, the diffusion rate gradually decreased (~10⁻¹¹ cm²/s) owing to fewer vacant sites for potassium association. Considering the high diffusion and excess of K₄Fe(CN)₆, the diffusion of $K_4 Fe(CN)_6$ is considered to remain high ($\sim 7 \times 10^{-6}$), ⁶⁸ suggesting that the diffusion of indigo analyte is the limiting step in the entire diffusion process; thus, the overall diffusion coefficient of the battery reflects the diffusion coefficient of the indigo slurry. These values (from 10^{-7} to 10^{-11} cm²/s) are comparable to those of the graphitic nanocarbon potassium storage material, calculated using the same method, suggesting that indigo has great potential as a K+ storage material. Compared with traditional carbon materials, indigo as an organic compound has remarkable advantages in terms of molecular malleability.69

In general, cyclability is one of the most important parameters for evaluating the lifetime and stability of a battery.

ACS Energy Letters http://pubs.acs.org/journal/aelccp Letter

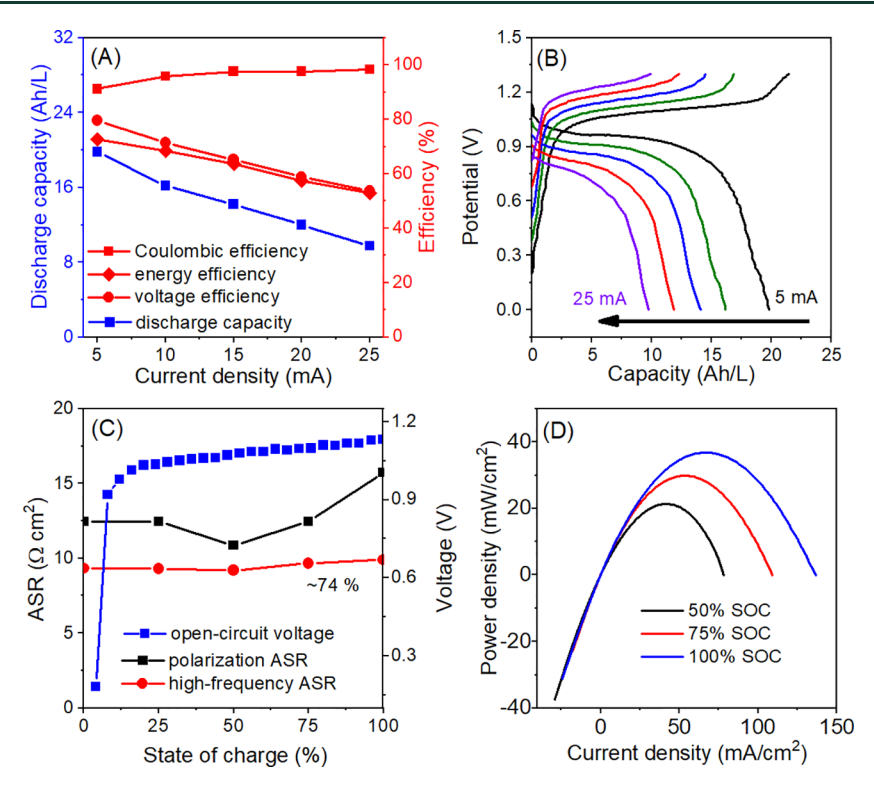


Figure 6. Polarization and rate ability of a 1.0 M indigo/ K_4 Fe(CN)₆ battery. (A) Coulombic efficiency, energy efficiency, voltage efficiency, and discharge capacity in the current range 5.0–25 mA. (B) Charge/discharge profiles at the current 5.0–25 mA. (C) High-frequency area specific resistance (ASR), polarization ASR, and open-circuit voltage of the battery vs state of charge (SOC). (D) Polarization of the battery at 50, 75, and 100% SOC.

The potassium storage performance of indigo was evaluated using a half-flow/half-slurry cell (Figures S5 and S6). In this study, to eliminate the potential effect of potassium ferricyanide degradation on battery performance, 68,70 excess $K_4Fe(CN)_6/K_3Fe(CN)_6$ was used as the catholyte to take full advantage of the indigo slurry (1.0 M indigo in 1.0 M KCl in H₂O/TEGDME stock solution). Before long-term cycling, KB was equilibrated and activated via a 20-cycle galvanostatic potentiostatic test (Figure S8). Prolonged galvanostatic cycling was performed to probe the cycling lifetime of the battery and the stability of indigo. The long-term cycling performance and selected galvanostatic discharge-charge profiles of the 1.0 M $(175 \text{ g/L}) \text{ indigo/} \text{K}_4\text{Fe}(\text{CN})_6 \text{ battery are shown in Figure 5A}$ and B, respectively, which present discharge/charge plateaus of approximately 1.1 V. The battery exhibited a high capacity of 18.4 Ah/L and a high-capacity retention of 82.8% over 1000 cycles, with an average capacity retention of 99.98% per cycle (Figure 5A). Compared with the reported slurry batteries, the proposed indigo/K₄Fe(CN)₆ full battery presents a medium to high capacity density, and the long-term stability is higher than most of the reported systems (Table S1).

Fourier-transform infrared (FT-IR) and UV-visible spectroscopic measurements were performed to explore the state of potassium insertion in the fully charged indigo anolyte. Precycling, after-charging, and postcycling indigo solutions in dimethyl sulfoxide (DMSO) were prepared for the FT-IR tests. An intense peak at 1709 cm^{-1} , ascribed to the carbonyl group, was observed before cycling that disappeared in the fully charged state, which supports the conclusion that the association of K^+ during the charging reaction broke the C= O carboxyl bond to afford oxygen anions for association with K^+ . The carbonyl peak at 1709 cm^{-1} was restored after

discharging, proving that the reaction of K⁺ at the carboxyl position is reversible during the charging and discharging process (Figure S9). The UV-visible absorption curves of precycling indigo exhibited an absorption peak at 619 nm (Figure S10).⁷² After charging, a new band originated from K⁺-associated indigo at 449 nm was observed.⁷³⁻⁷⁵ In addition, X-ray diffraction (XRD) on the indigo/KB slurry was also performed to confirm the indigo structural transformation during charging/discharging (Figures S11 and S12). The XRD pattern of the fully charged indigo slurry displayed a new crystal phase, as evidenced by the new signal pattern at 16°, 26°, and 28°. The identical XRD patterns before and after cycling also confirmed the indigo structural restoration during charging/discharging (Figure S12).

To gain insight into the possible side reactions and mechanism of capacity decay in the battery, a series of measurements was carried out on the postcycling battery and indigo slurry. As shown in Figure 5C, the bulk impedance (intercept at the x-axis in the high-frequency region in the EIS plot) increased from 5.1 Ω cm² to 5.6 Ω cm², due to blocking of the nanopores of the proton-exchange membrane by the conductive agent or indigo. However, the charge transfer impedance (the middle-frequency arc region) remained almost the same, indicating the superior electrochemical performance of indigo in aqueous electrolytes. The pre- and postcycling slurries were subjected to scanning electron microscope (SEM) and energy dispersive X-ray spectroscopy (EDS) measurements to gain information on the microstructure and element distribution in the slurry indigo anolyte (Figure S13). The SEM results suggest that indigo molecules are uniformly dispersed (Figure S13A), as the characteristic elements of indigo in this system, N and O, are evenly distributed without

aggregation (Figure S13E and G), and no concentrated distribution of C elements decoupled from N and O elements is observed (Figure S13C). This result also suggests the absence of KB aggregates. The microstructure of the slurry was maintained throughout the cycling process (Figure S13B, D, F, and H). In addition, the postcycling indigo was extracted with DMSO and subjected to CV measurements in tetrabutylammonium hexafluorophosphate (TBAPF₆)/DMSO electrolyte. The obtained current intensity in the CV scan was slightly reduced compared to that of the precycling slurry (Figure 5D), which is consistent with the capacity decay from the long-term cycling study. The ¹H NMR spectra of the electrolyte before and after cycling are shown in Figure S14. No additional peaks were found for the postcycling electrolyte, suggesting the stability of the indigo slurry. Low-concentration batteries (0.5 M) were also assembled and tested under the same conditions, and excellent long-cycle stability and high and stable Coulombic efficiency similar to that of the 1.0 M battery were also observed (Figure S15). A low-concentration indigo slurry battery (0.1 M) was assembled, where 73.8 mg of indigo/KB slurry (2.3 wt % of indigo) was used, corresponding to a two-electron theoretical capacity of 0.347 mAh. A low concentration is required for this study to ensure high-capacity utilization. During charging/discharging, this battery presented a charging capacity of 0.344 mAh and a discharging capacity of 0.304 mAh at a current density of 0.5 mA/cm², which suggests two-electron activity of indigo. In addition, only one charging/ discharging plateau was observed, supporting a one-step, twoelectron reaction mechanism (Figure S16).

The rate performance at different charge/discharge current densities largely reflects the electrochemical stability of the battery at high current densities. Traditionally, the undesired kinetic diffusivity of K+ in an organic solution severely limits the development of high-energy-density PIBs. In this study, the indigo battery was galvanostatically charged/discharged at current densities ranging from 5.0 to 25 mA (corresponding to \sim 3.5 to 17.2 mA/cm²) with an increment of 5.0 mA (Figure 6A). At each current density, the battery was cycled three times. At a relatively low current density of 5.0 mA, the battery delivered a discharge capacity of 19.8 Ah/L, corresponding to 51% of the theoretical capacity. Even at a high current density of 25 mA, the battery still presented a discharge capacity of 9.8. The charge/discharge profiles indicated that the overpotential of the battery increased with the current density (Figure 6B). Nevertheless, the battery exhibited high Coulombic efficiency (CE), energy efficiency (EE), and voltage efficiency (VE) (Figure 6C). At a current density of 5.0 mA, the CE, EE, and VE were 91.2, 79.6, and 72.6%, respectively. Even at 25 mA, the efficiencies were still 98.7, 53.7, and 52.9%, respectively.

The open-circuit voltage (OCV) is an important battery indicator that reflects both the initial properties of the active materials and the state of charge (SOC). In this indigo slurry battery, the OCV increased from 0.98 V at 12% SOC to 1.13 V at 100% SOC (Figure 6C), demonstrating a complete and stable charging platform for the battery at around 1.1 V. The high-frequency area specific resistance (ASR) (Figures 6C and S17), which originates from the separator, for accounted for about 74% of the polarization ASR. In addition, the polarization curves of the power density and current density (Figure 6D) exhibited a peak current power density of approximately 40 mW/cm².

The cost of indigo at the gram-scale is \$1280/kg according to Sigma Corporation, whereas the price of ton-scale

commercially available indigo is reduced to \$3.5/kg. To gain a more intuitive understanding, we compared the cost of indigo with those of 2,6-dihydroxy anthraquinone (DHAQ) and methyl viologen (MV), which are among the most promising and extensively studied analytes. 78-82 DHAQ has a small-batch cost of \$28800/kg according to Sigma Corporation and an estimated cost of \$4.74/kg on the large-scale. NV has a lab-scale cost of \$52000/kg according to Sigma Corporation and a large-scale cost of \$1/kg.83 When we broaden the cost considerations for the entire negative electrolyte (including the supporting salt and solution), unmodified anthraquinones require additional structural functionalization for property optimization and require highly basic solution (pH > 12) to achieve ideal performance.^{23,79,84} In contrast, pristine indigo can be directly used in a slurry system and is readily paired with a cost-effective catholyte, such as $K_4Fe(CN)_6$. Moreover, the supporting salt and solvents utilized in this slurry system are readily available at low cost (KCl \$0.2/kg, TEGDME/H₂O \$8/L). Thus, this indigo slurry battery is competitive with that employing the dominant anolyte organic material. Considering the cost of the entire battery (the pump, battery components and construction, piping, membrane, active material, and tank), we reduced the cost to \$306.5/kWh, according to the model in a previous work⁸⁵ (see the Supporting Information for more details).

In summary, an aqueous slurry battery employing a noncorrosive, cost-effective indigo anolyte was developed. Indigo readily achieved homogeneous dispersion and exhibited superior K⁺ diffusion capabilities. From the free-energy change of indigo during the charging/discharging process, the reaction was determined to be a one-step, double-electron process, rather than a two-step, single-electron process. The content of the conductive agent (KB in this case) had remarkable effects on the performance of the indigo/ K_4 Fe(CN)₆ battery. Ultimately, the designed indigo/K₄Fe(CN)₆ battery delivered excellent cycling performance over 1000 cycles with an average Coulombic efficiency of above 97.7% and capacity retention of 99.98% per cycle. This slurry strategy broadens the application of insoluble redox materials and overcomes the solubility limit of the energy density of the battery system. In addition, indigo has been proven to be an effective K+-storing organic material with great applicability in PIBs. While advantageous, the halfslurry/half-solution battery still suffers from high viscosity, exposing high challenges to allow for capacity scalability. Engineering of redox flow battery setups is urgently needed to further advance the development of slurry-based flow batteries.

ASSOCIATED CONTENT

Supporting Information

The Supporting Information is available free of charge at https://pubs.acs.org/doi/10.1021/acsenergylett.2c00165.

Computational methods, NMR spectrum of indigo, UV-vis spectrum of indigo, FTIR spectrum of indigo, cyclic voltammograms of indigo, and performance of the indigo battery (PDF)

AUTHOR INFORMATION

Corresponding Authors

Jingchao Chai – Department of Chemistry, University of Cincinnati, Cincinnati, Ohio 45221-0172, United States; Key Laboratory of Optoelectronic Chemical Materials and Devices, Ministry of Education, Jianghan University, Wuhan 430056, China; Email: chaijc@jhun.edu.cn

Jianbing Jimmy Jiang — Department of Chemistry, University of Cincinnati, Cincinnati, Ohio 45221-0172, United States; orcid.org/0000-0002-7466-522X; Email: jianbing.jiang@uc.edu

Authors

Xiao Wang – Department of Chemistry, University of Cincinnati, Cincinnati, Ohio 45221-0172, United States

Shu Zhang — Qingdao Industrial Energy Storage Research Institute, Qingdao Institute of Bioenergy and Bioprocess Technology, Chinese Academy of Sciences, Qingdao 266101, China

Bingbing Chen – Department of Energy Science and Engineering, Nanjing Tech University, Nanjing 211816, China

Ashwin Chaturvedi – Department of Chemistry, University of Cincinnati, Cincinnati, Ohio 45221-0172, United States

Guanglei Cui — Qingdao Industrial Energy Storage Research Institute, Qingdao Institute of Bioenergy and Bioprocess Technology, Chinese Academy of Sciences, Qingdao 266101, China; orcid.org/0000-0001-5987-7569

Complete contact information is available at: https://pubs.acs.org/10.1021/acsenergylett.2c00165

Notes

The authors declare no competing financial interest.

ACKNOWLEDGMENTS

This work is supported by the National Science Foundation under grant No. CBET-2112798 and the University of Cincinnati for startup funding.

REFERENCES

- (1) Larcher, D.; Tarascon, J. M. Towards Greener and More Sustainable Batteries for Electrical Energy Storage. *Nat. Chem.* **2015**, 7 (1), 19–29.
- (2) Jiang, Q.; Zhao, Y.; Zhang, X.; Yang, X.; Chen, Y.; Chu, Z.; Ye, Q.; Li, X.; Yin, Z.; You, J. Surface Passivation of Perovskite Film for Efficient Solar Cells. *Nature Phys.* **2019**, *13* (7), 460–466.
- (3) Chalamala, B. R.; Soundappan, T.; Fisher, G. R.; Anstey, M. R.; Viswanathan, V. V.; Perry, M. L. Redox Flow Batteries: An Engineering Perspective. *Proc. IEEE* **2014**, *102* (6), 976–999.
- (4) Park, M.; Ryu, J.; Wang, W.; Cho, J. Material Design and Engineering of Next-Generation Flow-Battery Technologies. *Nat. Rev. Mater.* **2017**, 2 (1), 16080.
- (5) Schrage, B. R.; Zhang, B.; Petrochko, S. C.; Zhao, Z.; Frkonja-Kuczin, A.; Boika, A.; Ziegler, C. J. Highly Soluble Imidazolium Ferrocene Bis(Sulfonate) Salts for Redox Flow Battery Applications. *Inorg. Chem.* **2021**, *60* (14), 10764–10771.
- (6) Zhao, Z.; Zhang, B.; Schrage, B. R.; Ziegler, C. J.; Boika, A. Investigations into Aqueous Redox Flow Batteries Based on Ferrocene Bisulfonate. ACS Appl. Energy Mater. 2020, 3 (10), 10270–10277.
- (7) Xu, G.; Shangguan, X.; Dong, S.; Zhou, X.; Cui, G. Formulation of Blended-Lithium-Salt Electrolytes for Lithium Batteries. *Angew. Chem., Int. Ed.* **2020**, 59 (9), 3400–3415.
- (8) Wang, H.; Cui, L.-F.; Yang, Y.; Sanchez Casalongue, H.; Robinson, J. T.; Liang, Y.; Cui, Y.; Dai, H. Mn₃O₄-Graphene Hybrid as a High-Capacity Anode Material for Lithium Ion Batteries. *J. Am. Chem. Soc.* **2010**, *132* (40), *13978*–13980.
- (9) Wang, H.; Yang, Y.; Liang, Y.; Robinson, J. T.; Li, Y.; Jackson, A.; Cui, Y.; Dai, H. Graphene-Wrapped Sulfur Particles as a

- Rechargeable Lithium-Sulfur Battery Cathode Material with High Capacity and Cycling Stability. Nano Lett. 2011, 11 (7), 2644-2647.
- (10) Luo, W.; Shen, F.; Bommier, C.; Zhu, H.; Ji, X.; Hu, L. Na-Ion Battery Anodes: Materials and Electrochemistry. *Acc. Chem. Res.* **2016**, 49 (2), 231–240.
- (11) Yabuuchi, N.; Kubota, K.; Dahbi, M.; Komaba, S. Research Development on Sodium-Ion Batteries. *Chem. Rev.* **2014**, *114* (23), 11636–11682.
- (12) Mao, M.; Gao, T.; Hou, S.; Wang, C. A Critical Review of Cathodes for Rechargeable Mg Batteries. *Chem. Soc. Rev.* **2018**, 47 (23), 8804–8841.
- (13) Zhang, Z.; Cui, Z.; Qiao, L.; Guan, J.; Xu, H.; Wang, X.; Hu, P.; Du, H.; Li, S.; Zhou, X.; Dong, S.; Liu, Z.; Cui, G.; Chen, L. Novel Design Concepts of Efficient Mg-Ion Electrolytes toward High-Performance Magnesium-Selenium and Magnesium-Sulfur Batteries. *Adv. Energy Mater.* 2017, 7 (11), 1602055.
- (14) Fan, L.; Liu, Q.; Xu, Z.; Lu, B. An Organic Cathode for Potassium Dual-Ion Full Battery. ACS Energy Lett. 2017, 2 (7), 1614–1620
- (15) Fan, L.; Ma, R.; Wang, J.; Yang, H.; Lu, B. An Ultrafast and Highly Stable Potassium-Organic Battery. *Adv. Mater.* **2018**, *30* (51), No. e1805486.
- (16) Deng, Q.; Pei, J.; Fan, C.; Ma, J.; Cao, B.; Li, C.; Jin, Y.; Wang, L.; Li, J. Potassium Salts of Para-Aromatic Dicarboxylates as the Highly Efficient Organic Anodes for Low-Cost K-Ion Batteries. *Nano Energy* **2017**, *33*, 350–355.
- (17) Yaroshevsky, A. Abundances of Chemical Elements in the Earth's Crust. *Geochem. Int.* **2006**, 44 (1), 48–55.
- (18) Turekian, K. K.; Wedepohl, K. H. Distribution of the Elements in Some Major Units of the Earth's Crust. *Geol. Soc. Am. Bull.* **1961**, 72 (2), 175–192.
- (19) Matsuda, Y.; Nakashima, H.; Morita, M.; Takasu, Y. Behavior of Some Ions in Mixed Organic Electrolytes of High Energy Density Batteries. *J. Electrochem. Soc.* **1981**, *128* (12), 2552.
- (20) Xiong, P.; Zhao, X.; Xu, Y. Nitrogen-Doped Carbon Nanotubes Derived from Metal-Organic Frameworks for Potassium-Ion Battery Anodes. *ChemSusChem* **2018**, *11* (1), 202–208.
- (21) Kwabi, D. G.; Ji, Y.; Aziz, M. J. Electrolyte Lifetime in Aqueous Organic Redox Flow Batteries: A Critical Review. *Chem. Rev.* **2020**, 120 (14), 6467–6489.
- (22) Kwabi, D. G.; Lin, K.; Ji, Y.; Kerr, E. F.; Goulet, M.-A.; De Porcellinis, D.; Tabor, D. P.; Pollack, D. A.; Aspuru-Guzik, A.; Gordon, R. G.; Aziz, M. J. Alkaline Quinone Flow Battery with Long Lifetime at pH 12. *Joule* **2018**, 2 (9), 1894–1906.
- (23) Lin, K.; Chen, Q.; Gerhardt, M. R.; Tong, L.; Kim, S. B.; Eisenach, L.; Valle, A. W.; Hardee, D.; Gordon, R. G.; Aziz, M. J. Alkaline Quinone Flow Battery. *Science* **2015**, 349 (6255), 1529–1532.
- (24) Huang, J.; Yang, Z.; Murugesan, V.; Walter, E.; Hollas, A.; Pan, B.; Assary, R. S.; Shkrob, I. A.; Wei, X.; Zhang, Z. Spatially Constrained Organic Diquat Anolyte for Stable Aqueous Flow Batteries. ACS Energy Lett. 2018, 3 (10), 2533–2538.
- (25) Hollas, A.; Wei, X.; Murugesan, V.; Nie, Z.; Li, B.; Reed, D.; Liu, J.; Sprenkle, V.; Wang, W. A Biomimetic High-Capacity Phenazine-Based Anolyte for Aqueous Organic Redox Flow Batteries. *Nat. Energy* **2018**, 3 (6), 508–514.
- (26) Huang, J.; Duan, W.; Zhang, J.; Shkrob, I. A.; Assary, R. S.; Pan, B.; Liao, C.; Zhang, Z.; Wei, X.; Zhang, L. Substituted Thiadiazoles as Energy-Rich Anolytes for Nonaqueous Redox Flow Cells. *J. Mater. Chem. A* **2018**, *6* (15), 6251–6254.
- (27) Hu, B.; Tang, Y.; Luo, J.; Grove, G.; Guo, Y.; Liu, T. L. Improved Radical Stability of Viologen Anolytes in Aqueous Organic Redox Flow Batteries. *Chem. Commun.* **2018**, *54* (50), 6871–6874.
- (28) Yan, Y.; Vaid, T. P.; Sanford, M. S. Bis(Diisopropylamino)-Cyclopropenium-Arene Cations as High Oxidation Potential and High Stability Catholytes for Non-Aqueous Redox Flow Batteries. *J. Am. Chem. Soc.* **2020**, *142* (41), 17564–17571.
- (29) Cabrera, P. J.; Yang, X.; Suttil, J. A.; Hawthorne, K. L.; Brooner, R. E. M.; Sanford, M. S.; Thompson, L. T. Complexes Containing

- Redox Noninnocent Ligands for Symmetric, Multielectron Transfer Nonaqueous Redox Flow Batteries. J. Phys. Chem. C 2015, 119 (28), 15882–15889.
- (30) Sevov, C. S.; Fisher, S. L.; Thompson, L. T.; Sanford, M. S. Mechanism-Based Development of a Low-Potential, Soluble, and Cyclable Multielectron Anolyte for Nonaqueous Redox Flow Batteries. J. Am. Chem. Soc. 2016, 138 (47), 15378–15384.
- (31) Hendriks, K. H.; Sevov, C. S.; Cook, M. E.; Sanford, M. S. Multielectron Cycling of a Low-Potential Anolyte in Alkali Metal Electrolytes for Nonaqueous Redox Flow Batteries. *ACS Energy Lett.* **2017**, 2 (10), 2430–2435.
- (32) Xia, L.; Long, T.; Li, W.; Zhong, F.; Ding, M.; Long, Y.; Xu, Z.; Lei, Y.; Guan, Y.; Yuan, D. Highly Stable Vanadium Redox-Flow Battery Assisted by Redox-Mediated Catalysis. *Small* **2020**, *16* (38), 2003321.
- (33) Parasuraman, A.; Lim, T. M.; Menictas, C.; Skyllas-Kazacos, M. Review of Material Research and Development for Vanadium Redox Flow Battery Applications. *Electrochim. Acta* **2013**, *101*, 27–40.
- (34) Shi, Y.; Eze, C.; Xiong, B.; He, W.; Zhang, H.; Lim, T.; Ukil, A.; Zhao, J. Recent Development of Membrane for Vanadium Redox Flow Battery Applications: A Review. *Appl. Energy* **2019**, 238, 202–224.
- (35) Zhang, Y.; Zuo, T.-T.; Popovic, J.; Lim, K.; Yin, Y.-X.; Maier, J.; Guo, Y.-G. Towards Better Li Metal Anodes: Challenges and Strategies. *Mater. Today* **2020**, *33*, 56–74.
- (36) Wu, F.; Maier, J.; Yu, Y. Guidelines and Trends for Next-Generation Rechargeable Lithium and Lithium-Ion Batteries. *Chem. Soc. Rev.* **2020**, 49 (5), 1569–1614.
- (37) Luo, J.; Hu, B.; Hu, M.; Zhao, Y.; Liu, T. L. Status and Prospects of Organic Redox Flow Batteries toward Sustainable Energy Storage. ACS Energy Lett. 2019, 4 (9), 2220–2240.
- (38) DeBruler, C.; Hu, B.; Moss, J.; Liu, X.; Luo, J.; Sun, Y.; Liu, T. L. Designer Two-Electron Storage Viologen Anolyte Materials for Neutral Aqueous Organic Redox Flow Batteries. *Chem.* **2017**, *3* (6), 961–978.
- (39) Deunf, E.; Poizot, P.; Lestriez, B. Aqueous Processing and Formulation of Indigo Carmine Positive Electrode for Lithium Organic Battery. *J. Electrochem. Soc.* **2019**, *166* (4), A747–A753.
- (40) Yao, M.; Kuratani, K.; Kojima, T.; Takeichi, N.; Senoh, H.; Kiyobayashi, T. Indigo Carmine: An Organic Crystal as a Positive-Electrode Material for Rechargeable Sodium Batteries. *Sci. Rep.* **2015**, *4*. 3650.
- (41) Yao, M.; Araki, M.; Senoh, H.; Yamazaki, S.-i.; Sakai, T.; Yasuda, K. Indigo Dye as a Positive-Electrode Material for Rechargeable Lithium Batteries. *Chem. Lett.* **2010**, *39* (9), 950–952.
- (42) Eustis, R.; Tsang, T. M.; Yang, B.; Scott, D.; Liaw, B. Y. Seeking Effective Dyes for a Mediated Glucose—Air Alkaline Battery/Fuel Cell. *J. Power Sources* **2014**, 248, 1133—1140.
- (43) Mukhopadhyay, A.; Zhao, H.; Li, B.; Hamel, J.; Yang, Y.; Cao, D.; Natan, A.; Zhu, H. Abundant Organic Dye as an Anolyte for Aqueous Flow Battery with Multielectron Transfer. *ACS Appl. Energy Mater.* **2019**, 2 (10), 7425–7437.
- (44) Plitzko, I.; Mohn, T.; Sedlacek, N.; Hamburger, M. Composition of Indigo Naturalis. *Planta. Med.* **2009**, *75* (8), 860–863.
- (45) Oh, S. H.; Lee, C. W.; Chun, D. H.; Jeon, J. D.; Shim, J.; Shin, K. H.; Yang, J. H. A Metal-Free and All-Organic Redox Flow Battery with Polythiophene as the Electroactive Species. *J. Mater. Chem. A* **2014**, 2 (47), 19994–19998.
- (46) Yan, W.; Wang, C.; Tian, J.; Zhu, G.; Ma, L.; Wang, Y.; Chen, R.; Hu, Y.; Wang, L.; Chen, T.; Ma, J.; Jin, Z. All-Polymer Particulate Slurry Batteries. *Nat. Commun.* **2019**, *10* (1), 2513.
- (47) Duduta, M.; Ho, B.; Wood, V. C.; Limthongkul, P.; Brunini, V. E.; Carter, W. C.; Chiang, Y. M. Semi-Solid Lithium Rechargeable Flow Battery. *Adv. Energy Mater.* **2011**, *1* (4), 511–516.
- (48) Wang, X.; Chai, J.; Jiang, J. Redox Flow Batteries Based on Insoluble Redox-Active Materials. A Review. *Nano Mater. Sci.* **2021**, 3 (1), 17–24.

- (49) Qi, Z.; Koenig, G. M. Review Article: Flow Battery Systems with Solid Electroactive Materials. *J. Vac. Sci. Technol. B* **2017**, 35 (4), 040801
- (50) Xing, X.; Liu, Q.; Li, J.; Han, Z.; Wang, B.; Lemmon, J. P. A Nonaqueous All Organic Semisolid Flow Battery. *Chem. Commun.* **2019**, 55 (94), 14214–14217.
- (51) Wei, J.; Zhang, P.; Liu, Y.; Liang, J.; Xia, Y.; Tao, A.; Zhang, K.; Tie, Z.; Jin, Z. Hypersaline Aqueous Lithium-Ion Slurry Flow Batteries. ACS Energy Lett. 2022, 7, 862–870.
- (52) Chen, H.; Zhou, Y.; Lu, Y.-C. Lithium—Organic Nanocomposite Suspension for High-Energy-Density Redox Flow Batteries. *ACS Energy Lett.* **2018**, 3 (8), 1991—1997.
- (53) Narayanan, A.; Wijnperlé, D.; Mugele, F.; Buchholz, D.; Vaalma, C.; Dou, X.; Passerini, S.; Duits, M. H. G. Influence of Electrochemical Cycling on the rheo-Impedance of Anolytes for Li-Based Semi Solid Flow Batteries. *Electrochim. Acta* **2017**, *251*, 388–395
- (54) Chen, H.; Lu, Y.-C. A High-Energy-Density Multiple Redox Semi-Solid-Liquid Flow Battery. *Adv. Energy Mater.* **2016**, *6* (8), 1502183.
- (55) He, X.; Yang, F.; Li, S.; He, X.; Yu, A.; Chen, J.; Xu, J.; Wang, J. Ultrafast Excited-State Intermolecular Proton Transfer in Indigo Oligomer. *J. Phys. Chem. A* **2019**, *123* (30), 6463–6471.
- (56) Frisch, M. J.; Trucks, G.; Schlegel, H.; Scuseria, G.; Robb, M.; Cheeseman, J.; Scalmani, G.; Barone, V.; Mennucci, B.; Petersson, G. *Gaussian 09*, Revision D.01; Gaussian, Inc.: Wallingford, CT, 2009.
- (57) Yang, F.; Mousavie, S. M. A.; Oh, T. K.; Yang, T.; Lu, Y.; Farley, C.; Bodnar, R. J.; Niu, L.; Qiao, R.; Li, Z. Sodium-Sulfur Flow Battery for Low-Cost Electrical Storage. *Adv. Energy Mater.* **2018**, 8 (11), 1701991.
- (58) Fan, F. Y.; Woodford, W. H.; Li, Z.; Baram, N.; Smith, K. C.; Helal, A.; McKinley, G. H.; Carter, W. C.; Chiang, Y. M. Polysulfide Flow Batteries Enabled by Percolating Nanoscale Conductor Networks. *Nano Lett.* **2014**, *14* (4), 2210–2218.
- (59) Lee, M.; Hong, J.; Lopez, J.; Sun, Y.; Feng, D.; Lim, K.; Chueh, W. C.; Toney, M. F.; Cui, Y.; Bao, Z. High-Performance Sodium-Organic Battery by Realizing Four-Sodium Storage in Disodium Rhodizonate. *Nat. Energy* **2017**, *2* (11), 861–868.
- (60) Zhao, J.; Zou, X.; Zhu, Y.; Xu, Y.; Wang, C. Electrochemical Intercalation of Potassium into Graphite. *Adv. Funct. Mater.* **2016**, 26 (44), 8103–8110.
- (61) Tang, S. B.; Lai, M. O.; Lu, L. Study on Li⁺ Ion Diffusion in Nano-Crystalline LiMn₂O₄ Thin Film Cathode Grown by Pulsed Laser Deposition Using CV, EIS and PITT Techniques. *Mater. Chem. Phys.* **2008**, *111* (1), 149–153.
- (62) Levi, M.; Salitra, G.; Markovsky, B.; Teller, H.; Aurbach, D.; Heider, U.; Heider, L. Solid-State Electrochemical Kinetics of Li-Ion Intercalation into Li_{1-x}CoO₂: Simultaneous Application of Electroanalytical Techniques SSCV, PITT, and EIS. *J. Electrochem. Soc.* **1999**, 146 (4), 1279.
- (63) Zhao, J.; Wang, L.; He, X.; Wan, C.; Jiang, C. Kinetic Investigation of LiCoO₂ by Electrochemical Impedance Spectroscopy (EIS). *Int. J. Electrochem. Sci.* **2010**, *5* (4), 478–488.
- (64) Tang, K.; Yu, X.; Sun, J.; Li, H.; Huang, X. Kinetic Analysis on LiFePO4 Thin Films by CV, GITT, and EIS. *Electrochim. Acta* **2011**, 56 (13), 4869–4875.
- (65) Taylor, S.; Gileadi, E. Physical Interpretation of the Warburg Impedance. Corrosion 1995, 51 (9), 664–671.
- (66) Kanoh, H.; Feng, Q.; Hirotsu, T.; Ooi, K. Ac Impedance Analysis for Li⁺ Insertion of a Pt/λ -MnO₂ Electrode in an Aqueous Phase. *J. Electrochem. Soc.* **1996**, *143* (8), 2610.
- (67) Huang, C.; Shen, C.; Jin, L.; Qu, D.; Hu, X.; Lin, Y.; Cai, H. The Determination of Trace Free Acid Content in Lithium-Ion Battery Electrolytes by Coulometric Titration in Non-Aqueous Media. *Analyst* **2020**, *145* (2), 582–587.
- (68) Luo, J.; Sam, A.; Hu, B.; DeBruler, C.; Wei, X.; Wang, W.; Liu, T. L. Unraveling pH Dependent Cycling Stability of Ferricyanide/Ferrocyanide in Redox Flow Batteries. *Nano Energy* **2017**, 42, 215–221.

- (69) Zhang, W.; Ming, J.; Zhao, W.; Dong, X.; Hedhili, M. N.; Costa, P. M. F. J.; Alshareef, H. N. Graphitic Nanocarbon with Engineered Defects for High-Performance Potassium-Ion Battery Anodes. *Adv. Funct. Mater.* **2019**, 29 (35), 1903641.
- (70) Long, Y.; Xu, Z.; Wang, G.; Xu, H.; Yang, M.; Ding, M.; Yuan, D.; Yan, C.; Sun, Q.; Liu, M. A Neutral Polysulfide/Ferricyanide Redox Flow Battery. *iScience* **2021**, *24* (10), 103157.
- (71) Sultana, I.; Rahman, M. M.; Wang, J.; Wang, C.; Wallace, G. G.; Liu, H.-K. Indigo Carmine (IC) Doped Polypyrrole (Ppy) as a Free-Standing Polymer Electrode for Lithium Secondary Battery Application. *Solid State Ion* **2012**, *215*, 29–35.
- (72) Franchi, D.; Calamante, M.; Coppola, C.; Mordini, A.; Reginato, G.; Sinicropi, A.; Zani, L. Synthesis and Characterization of New Organic Dyes Containing the Indigo Core. *Molecules* **2020**, 25 (15), 3377.
- (73) Bond, A. M.; Marken, F.; Hill, E.; Compton, R. G.; Hügel, H. The Electrochemical Reduction of Indigo Dissolved in Organic Solvents and as a Solid Mechanically Attached to a Basal Plane Pyrolytic Graphite Electrode Immersed in Aqueous Electrolyte Solution. J. Chem. Soc. 1997, 2 (9), 1735–1742.
- (74) Seixas de Melo, J.; Moura, A.; Melo, M. Photophysical and Spectroscopic Studies of Indigo Derivatives in Their Keto and Leuco Forms. *J. Phys. Chem. A* **2004**, *108* (34), 6975–6981.
- (75) Woodtli, P.; Giger, S.; Müller, P.; Sägesser, L.; Zucchetto, N.; Reber, M. J.; Ecker, A.; Brühwiler, D. Indigo in the Nanochannels of Zeolite L: Towards a New Type of Colorant. *Dyes Pigm* **2018**, *149*, 456–461.
- (76) Jin, S.; Jing, Y.; Kwabi, D. G.; Ji, Y.; Tong, L.; De Porcellinis, D.; Goulet, M.-A.; Pollack, D. A.; Gordon, R. G.; Aziz, M. J. A Water-Miscible Quinone Flow Battery with High Volumetric Capacity and Energy Density. ACS Energy Lett. 2019, 4 (6), 1342–1348.
- (77) Chai, J.; Lashgari, A.; Cao, Z.; Williams, C. K.; Wang, X.; Dong, J.; Jiang, J. PEGylation-Enabled Extended Cyclability of a Non-Aqueous Redox Flow Battery. ACS Appl. Energy Mater. 2020, 12 (13), 15262–15270.
- (78) Huskinson, B.; Marshak, M. P.; Suh, C.; Er, S.; Gerhardt, M. R.; Galvin, C. J.; Chen, X.; Aspuru-Guzik, A.; Gordon, R. G.; Aziz, M. J. A Metal-Free Organic-Inorganic Aqueous Flow Battery. *Nature* **2014**, 505 (7482), 195–198.
- (79) Hu, B.; Luo, J.; Hu, M.; Yuan, B.; Liu, T. L. A pH Neutral, Metal Free Aqueous Organic Redox Flow Battery Employing an Ammonium Anthraquinone Anolyte. *Angew. Chem., Int. Ed.* **2019**, 58, 16629–16636.
- (80) Ji, Y.; Goulet, M. A.; Pollack, D. A.; Kwabi, D. G.; Jin, S.; Porcellinis, D.; Kerr, E. F.; Gordon, R. G.; Aziz, M. J. A Phosphonate Functionalized Quinone Redox Flow Battery at near Neutral pH with Record Capacity Retention Rate. *Adv. Energy Mater.* **2019**, 9 (12), 1900039.
- (81) DeBruler, C.; Hu, B.; Moss, J.; Luo, J.; Liu, T. L. A Sulfonate-Functionalized Viologen Enabling Neutral Cation Exchange, Aqueous Organic Redox Flow Batteries toward Renewable Energy Storage. ACS Energy Lett. 2018, 3 (3), 663–668.
- (82) Luo, J.; Wu, W.; Debruler, C.; Hu, B.; Hu, M.; Liu, T. L. A 1.51 V pH Neutral Redox Flow Battery Towards Scalable Energy Storage. *J. Mater. Chem. A* **2019**, *7* (15), 9130–9136.
- (83) Hu, B.; DeBruler, C.; Rhodes, Z.; Liu, T. L. Long-Cycling Aqueous Organic Redox Flow Battery (AORFB) toward Sustainable and Safe Energy Storage. *J. Am. Chem. Soc.* **2017**, *139* (3), 1207–1214.
- (84) Chai, J.; Wang, X.; Lashgari, A.; Williams, C. K.; Jiang, J. A pH-Neutral, Aqueous Redox Flow Battery with a 3600-Cycle Lifetime: Micellization-Enabled High Stability and Crossover Suppression. *ChemSusChem* **2020**, *13* (16), 4069–4077.
- (85) Viswanathan, V.; Crawford, A.; Stephenson, D.; Kim, S.; Wang, W.; Li, B.; Coffey, G.; Thomsen, E.; Graff, G.; Balducci, P.; Kintner-Meyer, M.; Sprenkle, V. Cost and Performance Model for Redox Flow Batteries. *J. Power Sources* **2014**, *247*, 1040–1051.

☐ Recommended by ACS

Engineering Electrode/Electrolyte Interphase Chemistry toward High-Rate and Long-Life Potassium Ion Full-Cell

Ying Mo, Jilei Liu, et al.

ACS ENERGY LETTERS

READ 🗹

All-Organic Potassium Ion Hybrid Capacitor

Gudla Vardhini, Manikoth M. Shaijumon, et al.

AUGUST 08, 2022

ACS APPLIED ENERGY MATERIALS

READ 🗹

Correlation between Potassium-Ion Storage Mechanism and Local Structural Evolution in Hard Carbon Materials

Jia Xu, Jiantao Han, et al.

APRIL 18, 2022

CHEMISTRY OF MATERIALS

READ 🗹

Intercalation-Induced Conversion Reactions Give High-Capacity Potassium Storage

Jinzhi Sheng, Hui-Ming Cheng, et al.

OCTOBER 05, 2020

ACS NANO

READ 🗹

Get More Suggestions >